Applied Physics Letters

Vertical GaN p^+-n junction diode with ideal avalanche capability grown by halide vapor phase epitaxy

Cite as: Appl. Phys. Lett. **119**, 152102 (2021); https://doi.org/10.1063/5.0066139
Submitted: 08 August 2021 • Accepted: 28 September 2021 • Published Online: 12 October 2021

Kazuki Ohnishi, Seiya Kawasaki, Naoki Fujimoto, et al.

Applied Physics Letters ARTICLE scitation.org/journal/apl

Vertical GaN p^+-n junction diode with ideal avalanche capability grown by halide vapor phase epitaxy

Cite as: Appl. Phys. Lett. **119**, 152102 (2021); doi: 10.1063/5.0066139
Submitted: 8 August 2021 · Accepted: 28 September 2021 ·
Published Online: 12 October 2021

View Online Export Citation CrossMark

Kazuki Ohnishi,[1,a)] Seiya Kawasaki,[1] Naoki Fujimoto,[2] Shugo Nitta,[2] Hirotaka Watanabe,[2] Yoshio Honda,[2] and Hiroshi Amano[2,3,4]

AFFILIATIONS

[1]Graduate School of Engineering, Nagoya University, Nagoya 464-8603, Japan
[2]Institute of Materials and Systems for Sustainability, Nagoya University, Nagoya 464-8601, Japan
[3]Akasaki Research Center, Nagoya University, Nagoya 464-8603, Japan
[4]Venture Business Laboratory, Nagoya University, Nagoya 464-8603, Japan

[a)]Author to whom correspondence should be addressed: k.ohnishi@nagoya-u.jp

ABSTRACT

A vertical GaN p^+-n junction diode with an ideal breakdown voltage was grown by halide vapor phase epitaxy (HVPE). A steep p^+-n interface was observed even with the use of the HVPE method. No Si-accumulating layer was formed at the p^+-n interface because of the continuous HVPE growth from the n-type drift layer to the p-type layer. This method provides improved electrical properties compared with the regrowth of p-type GaN layers. The minimum ideality factor of approximately 1.6 was obtained. The breakdown voltage increased from 874 to 974 V with the increase in the temperature from 25 to 200 °C, which suggests that avalanche multiplication causes the breakdown. The temperature-dependent breakdown voltage was in good agreement with the breakdown voltage calculated using the ideal critical electric field. These results indicate that HVPE is promising for the fabrication of vertical GaN power devices.

The performance of silicon power devices has reached the material limit. For improving the performance of power devices and realizing carbon neutrality, gallium nitride (GaN), which is a major wide-bandgap semiconductor, is one of the key materials owing to its superior properties, such as its high breakdown electric field, high electron mobility, and high saturation velocity.[1–4] Commonly, GaN-based power-device structures have been grown by metalorganic vapor phase epitaxy (MOVPE).[5–11] MOVPE-grown GaN layers contain residual carbon impurity at the concentration of the order of 10^{15}–10^{16} cm^{-3}, originating from metalorganics used as group III precursors.[12,13] This carbon impurity compensates for carriers because it acts as not only a deep donor but also a deep acceptor.[13–17] To fabricate high-breakdown power devices, thick drift layers with a doping concentration of less than 10^{16} cm^{-3} are required. To grow drift layers with low doping concentrations by MOVPE, the growth rate must be as low as 2–4 μm/h to suppress the incorporation of a carbon impurity.[12] Thus, it is difficult to grow thick GaN drift layers with low doping concentration by MOVPE.

Halide vapor phase epitaxy (HVPE), which is well known as the growth method for free-standing GaN substrates,[18,19] is effective for fabricating vertical GaN power devices, such as the Schottky barrier diode and p-n junction diode (PND). This is because the HVPE method uses carbon-free sources, which are GaCl and/or $GaCl_3$, as the Ga precursor and its typical growth rate is higher than 100 μm/h. These features are suitable for growing thick GaN drift layers with a low doping concentration. Despite being an attractive method for fabricating vertical power devices, there are a few reports on applying the HVPE method to device fabrication because of the incorporation of residual impurities, such as Si and O in unintentionally doped GaN layers and the difficulty in fabricating p-type GaN layers.[20–22] In recent years, residual Si and O concentrations ([Si] and [O]) of the order of 10^{14} cm^{-3} and the reduction in the density of major electron traps have been realized by using a quartz-free HVPE reactor.[3,23–25] On the other hand, the fabrication of p-type GaN layers by HVPE is difficult and the vertical GaN PND has not been fabricated by HVPE. Hence, the vertical GaN PND has been fabricated by a hybrid HVPE method in which the MOVPE and HVPE methods are combined: The n-type and p-type GaN layers are grown by HVPE and MOVPE, respectively.[21] The regrowth interface commonly contains Si impurity at

high concentrations,[26–29] and this Si-accumulating layer seriously affects the electrical properties of p-n diodes.[21,28,29] Fu and coworkers reported that this contamination could enhance the local electrical field and cause the high leakage current and a premature breakdown of devices.[28,29] They also reported that a specific surface state of GaN, such as nitrogen vacancy, gallium dangling bonds, and/or oxidation, could enhance the Si adsorption.[29] However, the origin of the Si-accumulating layer at the regrowth interface has been unclear and the elimination method has not been established. For fabricating vertical GaN PNDs by HVPE without Si contaminations at the p-n interface, the continuous HVPE growth of the p-type GaN layer is favorable. Recently, we have established a method of the HVPE growth of p-type GaN layers,[30,31] making it possible to fabricate a vertical GaN PND without Si contamination. In this study, we report on the HVPE growth of a vertical PND on a free-standing n^+-GaN substrate and the electrical properties of devices. The fabricated vertical PND showed avalanche breakdown, and the breakdown voltage was in good agreement with the value calculated on the basis of the ideal critical electrical field from Ref. 2.

A schematic of the fabricated vertical GaN PND is shown in Fig. 1. This PND structure was grown by HVPE on a free-standing n^+-type GaN substrate. The free-standing GaN substrate grown by HVPE has the threading dislocation density of $1.7 \times 10^6\,cm^{-2}$ and the carrier concentration of $1.5 \times 10^{18}\,cm^{-3}$ as indicated by the wafer supplier. First, an approximately 200-nm-thick n^+-type GaN layer was grown on the n^+-type GaN free-standing substrate. Then, a 15-μm-thick n-type GaN drift layer with [Si] of $3 \times 10^{16}\,cm^{-3}$ was grown. The growth rate of the n-type GaN drift layer was set to 30 μm/h. As the Ga precursor, GaCl gas, which was formed by the reaction between Ga melt and HCl gas at 900 °C, was used. NH_3 gas was used as the N precursor. The HCl flow rate in Ga melt and the NH_3 flow rate were 40 sccm and 4 slm, respectively. For Si doping, $SiCl_4$ gas was used. After the growth of the n-type GaN drift layer, the growth rate was set to approximately 3 μm/h by reducing the flow rate of the input HCl gas in Ga melt to 4 sccm to grow the Mg-doped GaN layer. An approximately 300-nm-thick Mg-doped GaN layer with the Mg concentration ([Mg]) of $2 \times 10^{19}\,cm^{-3}$ was grown. Finally, an approximately 20-nm-thick heavily Mg-doped contact layer was grown by

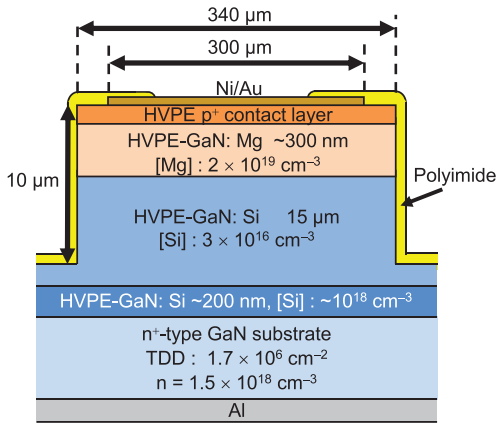

FIG. 1. Schematic cross section of the vertical GaN p^+-n junction diode grown by HVPE. Polyimide was coated for passivation.

HVPE continuously. In the case of Mg doping, MgO solid was used as a Mg doping source.[30,31] In a thermodynamic calculation, $MgCl_2$ gas is mainly formed by the reaction between MgO solid and HCl gas.[32] Hence, a Mg precursor is delivered as $MgCl_2$ formed by reacting MgO solid with HCl at 900 °C. Details of the Mg doping method and thermodynamic mechanism are described in Refs. 30 and 32, respectively. Throughout the HVPE growth, the growth temperature and pressure were kept at 1050 °C and 1 atm, respectively. After the HVPE growth of the PND structure, the PND was fabricated. For the edge termination, the vertical deep mesa structure was formed by inductively coupled plasma-reactive ion etching. The etching depth was 10 μm. The mesa diameter was 340 μm. To activate Mg acceptors, the sample was annealed at 700 °C in nitrogen ambient for 5 min. The anode was alloyed Ni/Au on the p^+-type contact layer. The cathode was Al formed on the back of the free-standing n^+-type GaN substrate. The 3-μm-thick polyimide was coated to passivate the sidewall. Details of the fabrication process were described in Refs. 33 and 34.

To confirm whether the p^+-n junction was formed by HVPE, a cross-sectional observation and analysis of the depth profile of impurity concentrations of an as-grown vertical GaN PND structure were performed by scanning electron microscopy (SEM) and secondary ion mass spectrometry (SIMS), respectively. Figure 2(a) shows a cross-sectional SEM image of the as-grown vertical GaN PND structure. The bright and dark contrast layers, which were p-type and n-type GaN layers, respectively, are clearly observed, suggesting that the p-n interface can be clearly discriminated. The thickness of the p-type GaN layer was approximately 300 nm, and the thickness distribution of the p-type GaN layer was very small. It is possible to control the thickness within ~300 nm even by the HVPE method, which has a higher growth rate than the MOVPE method. The SIMS depth profiles of [Si], [O], [Mg], C, and H concentrations ([C] and [H]) of the as-grown vertical GaN PND structure are shown in Fig. 2(b). [O], [C], and [H] in the n-type GaN drift layer were lower than the detection limits (7×10^{15}, 3×10^{15}, and $3 \times 10^{15}\,cm^{-3}$, respectively). The average [Si] in the n-type GaN drift layer was $3 \times 10^{16}\,cm^{-3}$. For the hybrid PND from Ref. 21, Si atoms accumulated at the p-n interface owing to the regrowth of the p-type GaN layer by MOVPE, whereas no Si-accumulating layer was successfully formed at the p-n interface in our sample because of the continuous HVPE growth. [H] in the p-type GaN layer was comparable to [Mg] in the as-grown sample. This is because Mg atoms are passivated with H atoms in as-grown Mg-doped GaN layers by HVPE, the same as in MOVPE-grown samples.[30] [Mg] sharply increased from $5 \times 10^{15}\,cm^{-3}$ in the n-type GaN drift layer to $1.9 \times 10^{19}\,cm^{-3}$ in the p-type GaN layer at the p^+-n interface, indicating the HVPE growth of a steep p^+-n interface is possible. The thickness of the transition layer from n-type GaN to p^+-type GaN was approximately 200 nm. Further improvement in the supplying of Mg precursors is important for growing the steeper p-n interface.

The capacitance–voltage (C–V) measurement was performed to determine the built-in voltage of the p^+-n junction and the net donor concentration ($N_{net} = N_d - N_a$, N_d, donor concentration; N_a, acceptor concentration) in the drift region. Figure 3(a) shows the $1/C^2$–V plot of the vertical GaN PND. The measurement frequency was 100 kHz. From the intercept of the $1/C^2$–V plot, the built-in voltage was 3.2 V. The depth-dependent N_{net} calculated from the C–V characteristics in Fig. 3(a) is shown in Fig. 3(b). The average N_{net} was $2.3 \times 10^{16}\,cm^{-3}$.

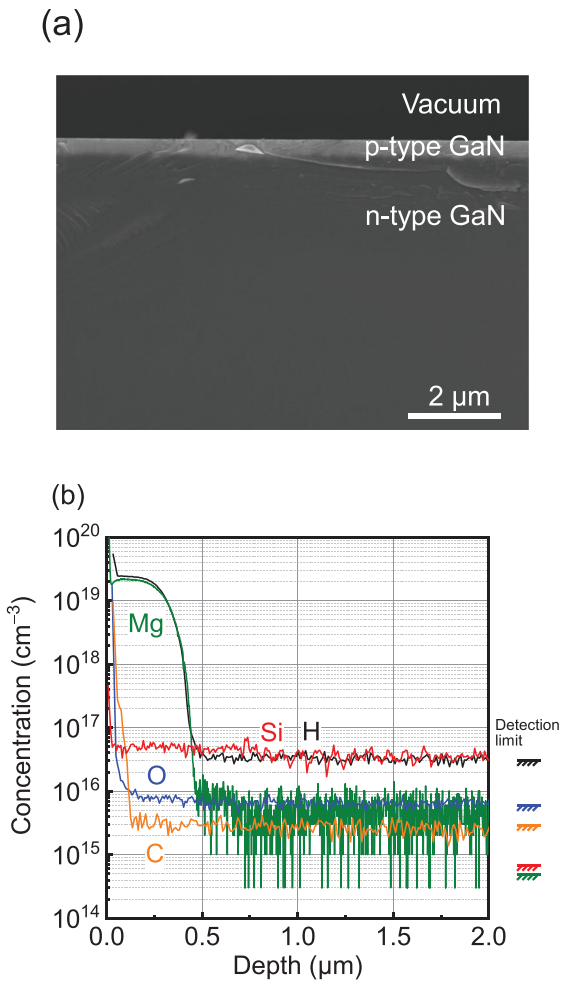

FIG. 2. (a) Cross-sectional SEM image of as-grown p$^+$-n junction diode structure. (b) SIMS depth profiles of Si, O, C, H, and Mg concentrations for the as-grown vertical GaN p$^+$-n junction diode structure.

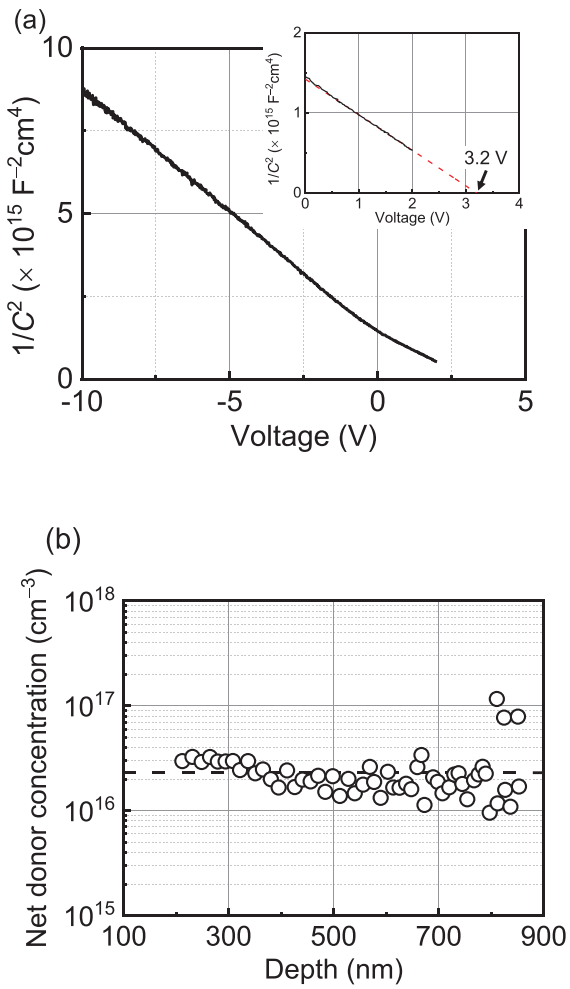

FIG. 3. (a) $1/C^2$–V plot of the vertical GaN p$^+$-n junction diode measured at 100 kHz. Inset: the magnification of plot from 0 to 4 V. (b) Net donor concentration vs depletion depth extracted from C–V characteristics. The dashed line is the average N_{net}, which is 2.3×10^{16} cm^{-3}.

The obtained built-in potential, which was 3.2 V, is in good agreement with the average N_{net} in the drift layer of the PND. In the drift layer, [O] was lower than the detection limit, as already mentioned. Thus, [Si] can be considered equal to N_d. N_{net} was slightly lower than N_d in the drift layer. The residual [Mg] in the drift layer was 5×10^{15} cm^{-3}. If the Mg atoms compensate for donors as acceptors, i.e., $[Mg] = N_a$, the difference between N_d and [Mg] corresponds to N_{net}. This residual Mg concentration is due to the Mg memory effect like MOVPE.[35] Mg atoms with the concentration of 10^{15} cm^{-3} remain after the Mg doping in the HVPE system. Further improvement in the baking condition of the HVPE system could lead to the elimination of residual Mg atoms in n-type GaN drift layers.

Figure 4 shows the forward current–voltage (J–V) characteristic of the vertical GaN PND at 298 K. The ideality factor n [$n = e/\{kT(\mathrm{d}\ln(J)/\mathrm{d}V)\}$, where e, k, and T are the electrical charge, Boltzmann constant, and temperature, respectively] is also shown in Fig. 4. The minimum n value was approximately 1.6, which is similar to or slightly larger than those in previous reports grown by MOVPE ($n = 1.1$–2.3).[9,10,33,36–38] This n value of vertical GaN PND was also lower than that of hybrid PND composing a combination of HVPE and MOVPE.[21] The improvement in the n value is to be due to the adequate suppression of Si accumulation at the p$^+$-n interface by continuous HVPE growth, as shown in Fig. 2(b). To confirm the breakdown of the vertical GaN PND, reverse J–V characteristics were measured at various device temperature from 25 to 200 °C. The temperature dependence of reverse J–V characteristics is shown in Fig. 5. Nondestructive breakdown was observed in the temperature range of 25 to 200 °C, and the breakdown voltage increased from 874 to 974 V with increasing temperature. When the breakdown is caused by avalanche multiplication, the breakdown voltage increases with the increasing temperature. This is because the phonon scattering rate in a semiconductor increases, and it is too difficult to obtain sufficient energy of carriers to cause impact ionization with the increasing temperature. Thus, the nondestructive breakdown in the vertical GaN PND grown by HVPE suggests an avalanche breakdown. Figure 6

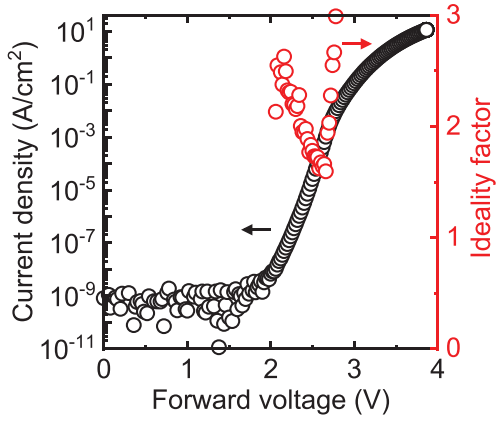

FIG. 4. Forward *J–V* characteristics and voltage dependence of the ideality factor in the vertical GaN p$^+$-n junction diode.

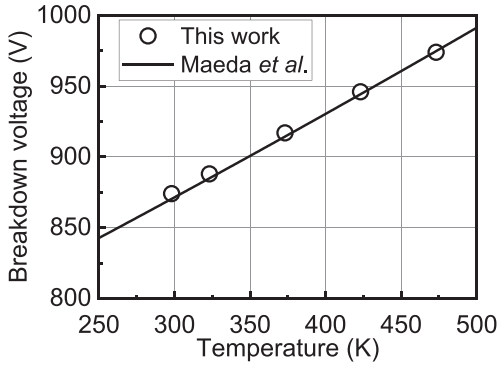

FIG. 6. Temperature dependence of breakdown voltage of the vertical GaN p$^+$-n junction diode. The experimental data are plotted as dots. The solid line indicates the ideal breakdown voltage calculated using Eq. (9) from Ref. 2 with N_{net} of 2.3×10^{16} cm^{-3}.

shows the temperature dependence of breakdown voltage. The breakdown voltage almost linearly increased with the increasing temperature. Recently, Maeda *et al.* reported the impact ionization coefficients of electrons and holes in GaN and the critical electric field for a GaN p$^+$-n junction under the non-punch-thorough (NPT) condition.[2] Our vertical GaN PND grown by HVPE was fabricated under the NPT condition. Hence, the breakdown voltage based on the critical electrical field in Eq. (9) from Ref. 2 was calculated with the N_{net} value of 2.3×10^{16} cm^{-3}. The solid line is the calculated breakdown voltage from Ref. 2. The experimental data are in good agreement with the solid line, indicating that the HVPE-grown vertical GaN PND has the ideal critical electrical field and avalanche capability. Figure 7 shows the breakdown voltage as a function of doping concentration. Red circle shows the experimental data of the HVPE-grown vertical GaN PND. The other plots are the reported experimental values of GaN PNDs grown by MOVPE.[10,11,33,37–41] The solid line indicates the ideal breakdown for GaN p$^+$-n junction under the NPT condition from Ref. 2. The breakdown voltage of the HVPE-grown PND follows the ideal value. By further reducing the doping concentration in HVPE-grown thick GaN drift layers, it is possible to fabricate vertical PNDs with higher breakdown voltage.

As described above, the HVPE-grown vertical GaN PND has the ideal avalanche capability. However, the reverse leakage current was higher than that of a similar device grown by MOVPE.[33,34] This reverse leakage current was also observed in other devices with different device diameters, and this leakage mechanism has been under investigation. To investigate where the current leakage occurred, we performed the emission microscopy under the reverse voltage lower than the avalanche breakdown. This microscopy can detect the current leakage as light emission.[33,34,38,42] Dotlike leakage spots into the device were observed when applying reverse voltage and the impact of the leakage from the sidewall was small. In the case of MOVPE-grown GaN PNDs, Usami and coworkers reported that the pure screw

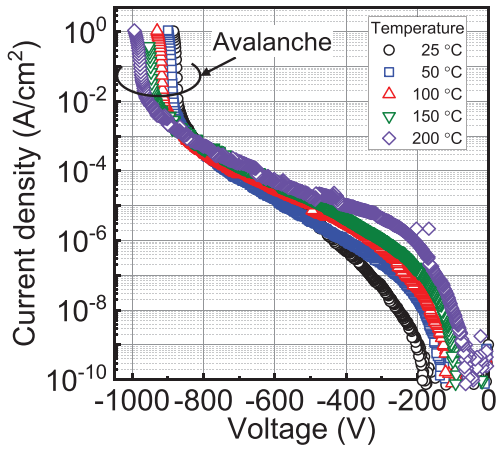

FIG. 5. Temperature dependence of reverse *J–V* characteristics of the vertical GaN p$^+$-n junction diode. The avalanche breakdown voltage increased with increasing temperature.

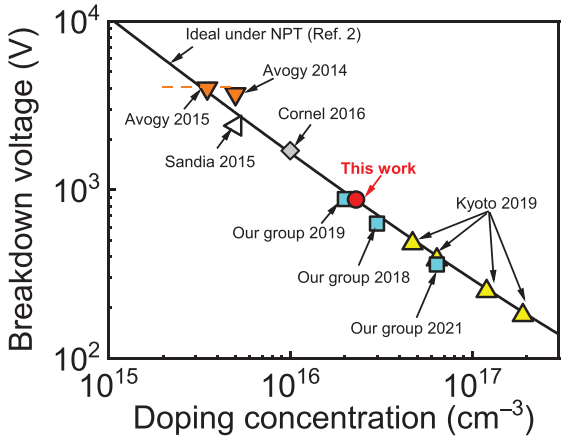

FIG. 7. Breakdown voltage as a function of doping concentration reported GaN PNDs. The solid line indicates the ideal breakdown voltage for the GaN p$^+$—n junction under the NPT condition calculated by Ref. 2. Red circle shows the experimental data of this work. The other plots are the reported experimental values of GaN PNDs grown by MOVPE.[10,11,33,37–41] The dashed line indicates the doping concentration range in Ref. 11.

dislocations were related to the reverse leakage current and that the improvement of the MOVPE growth conditions suppressed the reverse leakage.[38,42] The reverse J–V characteristics shown in Fig. 5 are similar to those in MOVPE-grown GaN PNDs with large leakage current in Ref. 42. It is unclear whether the origin of the reverse leakage between MOVPE- and HVPE-grown GaN PNDs is common or not because of the different growth methods used. Further investigation of the origin of the reverse leakage in HVPE-grown vertical GaN PNDs and the suppression of the reverse leakage are needed and will be reported elsewhere.

In summary, we fabricated a vertical GaN PND with the ideal avalanche capability grown by HVPE. The steep p^+-n interface without Si accumulation can be grown by continuous HVPE growth, which is superior to the hybrid growth by the combination of MOVPE and HVPE in terms of obtaining the ideal breakdown voltage and low forward leakage current. The minimum n value, which was approximately 1.6, was similar to or slightly higher than that of previously reported PNDs grown by MOVPE. We obtained the avalanche breakdown by evaluating the temperature dependence of the reverse J–V characteristics. The temperature dependence of breakdown voltage shows that the breakdown in the HVPE-grown vertical GaN PND is caused by ideal avalanche multiplication. According to the results of this study, the HVPE method is a promising technique for the growth of vertical p-n junction GaN device structures.

This research was supported by MEXT-Program for Creation of Innovative Core Technology for Power Electronics Program under Grant No. JPJ009777 and JSPS KAKENHI under Grant No. 20J13885.

DATA AVAILABILITY

The data that support the findings of this study are available from the corresponding author upon reasonable request.

REFERENCES

[1]T. Kachi, Jpn. J. Appl. Phys., Part 1 **53**, 100210 (2014).
[2]T. Maeda, T. Narita, S. Yamada, T. Kachi, T. Kimoto, M. Horita, and J. Suda, J. Appl. Phys. **129**, 185702 (2021).
[3]H. Fujikura, T. Konno, T. Kimura, Y. Narita, and F. Horikiri, Appl. Phys. Lett. **117**, 012103 (2020).
[4]J. Kolník, İH. Oğuzman, K. F. Brennan, R. Wang, P. P. Ruden, and Y. Wang, J. Appl. Phys. **78**, 1033 (1995).
[5]Y. Saitoh, K. Sumiyoshi, M. Okada, T. Horii, T. Miyazaki, H. Shiomi, M. Ueno, K. Katayama, M. Kiyama, and T. Nakamura, Appl. Phys. Express **3**, 081001 (2010).
[6]W. Li, K. Nomoto, M. Pilla, M. Pan, X. Gao, D. Jena, and H. G. Xing, IEEE Trans. Electron Devices **64**, 1635 (2017).
[7]M. Kanechika, M. Sugimoto, N. Soejima, H. Ueda, O. Ishiguro, M. Kodama, E. Hayashi, K. Itoh, T. Uesugi, and T. Kachi, Jpn. J. Appl. Phys., Part 2 **46**, L503 (2007).
[8]T. Oka, T. Ina, Y. Ueno, and J. Nishii, Appl. Phys. Express **8**, 054101 (2015).
[9]H. Hatakeyama, K. Nomoto, N. Kaneda, T. Kawano, T. Mishima, and T. Nakamura, IEEE Electron Device Lett. **32**, 1674 (2011).
[10]K. Nomoto, B. Song, Z. Hu, M. Zhu, M. Qi, N. Kaneda, T. Mishima, T. Nakamura, D. Jena, and H. G. Xing, IEEE Electron Device Lett. **37**, 161 (2016).
[11]I. C. Kizilyalli, T. Prunty, and O. Aktas, IEEE Electron Device Lett. **36**, 1073 (2015).
[12]G. Piao, K. Ikenaga, Y. Yano, H. Tokunaga, A. Mishima, Y. Ban, T. Tabuchi, and K. Matsumoto, J. Cryst. Growth **456**, 137 (2016).
[13]N. Sawada, T. Narita, M. Kanechika, T. Uesugi, T. Kachi, M. Horita, T. Kimoto, and J. Suda, Appl. Phys. Express **11**, 041001 (2018).
[14]J. L. Lyons, A. Janotti, and C. G. Van de Walle, Appl. Phys. Lett. **97**, 152108 (2010).
[15]D. O. Demchenko, I. C. Diallo, and M. A. Reshchikov, Phys. Rev. Lett. **110**, 087404 (2013).
[16]J. L. Lyons, A. Janotti, and C. G. Van de Walle, Phys. Rev. B **89**, 035204 (2014).
[17]T. Narita, K. Tomita, Y. Tokuda, T. Kogiso, M. Horita, and T. Kachi, J. Appl. Phys. **124**, 215701 (2018).
[18]K. Fujito, S. Kubo, H. Nagaoka, T. Mochizuki, H. Namita, and S. Nagao, J. Cryst. Growth **311**, 3011 (2009).
[19]H. Fujikura, T. Yoshida, M. Shibata, and Y. Otoki, Proc. SPIE **10104**, 1010403 (2017).
[20]R. P. Tompkins, M. R. Khan, R. Green, K. A. Jones, and J. H. Leach, J. Mater. Sci.: Mater. Electron. **27**, 6108 (2016).
[21]H. Fujikura, K. Hayashi, F. Horikiri, Y. Narita, T. Konno, T. Yoshida, H. Ohta, and T. Mishima, Appl. Phys. Express **11**, 045502 (2018).
[22]P. Kruszewski, P. Prystawko, M. Grabowski, T. Sochacki, A. Sidor, M. Bockowski, J. Jasinski, L. Lukasiak, R. Kisiel, and M. Leszczynski, Mater. Sci. Semicond. Process **96**, 132 (2019).
[23]H. Fujikura, T. Konno, T. Yoshida, and F. Horikiri, Jpn. J. Appl. Phys., Part 1 **56**, 085503 (2017).
[24]K. Kanegae, H. Fujikura, Y. Otoki, T. Konnno, T. Yoshida, M. Horita, T. Kimoto, and J. Suda, Appl. Phys. Lett. **115**, 012103 (2019).
[25]T. Kimura, T. Konnno, and H. Fujikura, Appl. Phys. Lett. **118**, 182104 (2021).
[26]H. Xing, S. P. DenBaars, and U. K. Mishra, J. Appl. Phys. **97**, 113703 (2005).
[27]G. Koblmüller, R. M. Chu, A. Raman, U. K. Mishra, and J. S. Speck, J. Appl. Phys. **107**, 043527 (2010).
[28]K. Fu, H. Fu, H. Liu, S. R. Alugubelli, T.-H. Yang, X. Huang, H. Chen, I. Baranowski, J. Montes, F. A. Ponce, and Y. Zhao, Appl. Phys. Lett. **113**, 233502 (2018).
[29]K. Fu, H. Fu, X. Deng, P.-Y. Su, H. Liu, K. Hatch, C.-Y. Cheng, D. Messina, R. V. Meidanshahi, P. Peri, C. Yang, T.-H. Yang, J. Montes, J. Zhou, X. Qi, S. M. Goodnick, F. A. Ponce, D. J. Smith, R. Nemanich, and Y. Zhao, Appl. Phys. Lett. **118**, 222104 (2021).
[30]K. Ohnishi, Y. Amano, N. Fujimoto, S. Nitta, Y. Honda, and H. Amano, Appl. Phys. Express **13**, 061007 (2020).
[31]K. Ohnishi, Y. Amano, N. Fujimoto, S. Nitta, H. Watanabe, Y. Honda, and H. Amano, J. Cryst. Growth **566–567**, 126173 (2021).
[32]T. Kimura, K. Ohnishi, Y. Amano, N. Fujimoto, M. Araidai, S. Nitta, Y. Honda, H. Amano, and K. Shiraishi, Jpn. J. Appl. Phys., Part 1 **59**, 088001 (2020).
[33]H. Fukushima, S. Usami, M. Ogura, Y. Ando, A. Tanaka, M. Deki, M. Kushimoto, S. Nitta, Y. Honda, and H. Amano, Appl. Phys. Express **12**, 026502 (2019).
[34]H. Fukushima, S. Usami, M. Ogura, Y. Ando, A. Tanaka, M. Deki, M. Kushimoto, S. Nitta, Y. Honda, and H. Amano, Jpn. J. Appl. Phys., Part 1 **58**, SCCD25 (2019).
[35]Y. Ohba and A. Hatano, J. Cryst. Growth **145**, 214 (1994).
[36]Z. Hu, K. Nomoto, B. Song, M. Zhu, M. Qi, M. Pan, X. Gao, V. Protasenko, D. Jena, and H. G. Xing, Appl. Phys. Lett. **107**, 243501 (2015).
[37]J. R. Dickerson, A. A. Allerman, B. N. Bryant, A. J. Fischer, M. P. King, M. W. Moseley, A. M. Armstrong, R. J. Kaplar, I. C. Kizilyalli, O. Aktas, and J. Wierer, IEEE Trans. Electron Devices **63**, 419 (2016).
[38]S. Usami, Y. Ando, A. Tanaka, K. Nagamatsu, M. Deki, M. Kushimoto, S. Nitta, Y. Honda, H. Amano, Y. Sugawara, Y.-Z. Yao, and Y. Ishikawa, Appl. Phys. Lett. **112**, 182106 (2018).
[39]S. Kawasaki, Y. Ando, M. Deki, H. Watanabe, A. Tanaka, S. Nitta, Y. Honda, M. Arai, and H. Amano, Appl. Phys. Express **14**, 046501 (2021).
[40]I. C. Kizilyalli, A. P. Edwards, H. Nie, D. Bour, T. Prunty, and D. Disney, IEEE Elecron Device Lett. **35**, 247 (2014).
[41]T. Maeda, T. Narita, H. Ueda, M. Kanechika, T. Uesugi, T. Kachi, T. Kimoto, M. Horita, and J. Suda, in *IEDM Technical Digest* (IEEE, 2018), pp. 30.1.1.
[42]S. Usami, A. Tanaka, H. Fukushima, Y. Ando, M. Deki, S. Nitta, Y. Honda, and H. Amano, Jpn. J. Appl. Phys., Part 1 **58**, SCCB24 (2019).